Isam Mejbel Abed
Professor
Department of Mechanical Engineering, College of Engineering, University of Babylon, Iraq

Ammar Abdulkadhim
Assistant Lecturer
Air Conditioning and Refrigeration Techniques, Engineering Department, Al-Mustaqbal University College, Babylon, Iraq

Ruqaia A. Hamzah
Assistant Lecturer
Air Conditioning and Refrigeration Techniques, Engineering Department, Al-Mustaqbal University College, Babylon, Iraq

Hammed K. Hamzah
Assistant Professor
Department of Mechanical Engineering, College of Engineering, University of Babylon, Iraq

Farooq H. Ali
Assistant Professor
Department of Mechanical Engineering, College of Engineering, University of Babylon, Iraq

Natural Convection Heat Transfer for Adiabatic Circular Cylinder Inside Trapezoidal Enclosure Filled with Nanofluid Superposed Porous–Nanofluid Layer

Heat transfer by natural convection for a centered inner adiabatic circular cylinder inside a trapezoidal enclosure filled with Ag–water nanofluid superposed saturated porous–nanofluid layer is numerically investigated. The inclined left and right walls of the trapezoidal enclosure are insulated. The bottom wall is partially heated at isotherm hot temperature, while the top wall is maintained at isotherm cold temperature. Finite element technique is used to numerically solve dimensionless Navier–Stoke equations for the nanofluid and porous–nanofluid media between inner adiabatic circular cylinder and trapezoidal enclosure. The numerical results are validated with those of Kim et al. [2008] in terms of streamlines and isotherms to check the accuracy of the present program. The validation illustrates a favorable agreement between the present work and Kim et al. The following parameters are studied: Rayleigh number ($10^3 \leq Ra \leq 10^6$), Darcy number ($10^{-1} \geq Da \geq 10^{-5}$), nanoparticle volume fraction ($0 \leq \varphi \leq 0.1$), and porous layer thickness ($0 \leq Yp \leq 100\%$).

Keywords: *natural convection, nanofluid, trapezoidal enclosure, porous media, finite element technique.*

1. INTRODUCTION

Natural heat transfer has gained importance in the last three decades for its various applications, such as cooling electronic devices and reducing energy leakage from energy conservation storages [1–4]. Aydin et al. [5] used the stream function-vorticity formulation to study the effect of aspect ratio within rectangular enclosures. They found that the effects of Rayleigh number and aspect ratio on heat transfer were more significant and stronger, respectively, when the enclosure was shallow. Specifically, when the enclosure was tall, the Rayleigh number was high. Basak et al. [6, 7] used a square cavity to study the influence of distributed heating on natural convection. They showed that thermal mixing and heat distribution inside a square cavity were highly enhanced compared to those in the isothermal hot bottom wall. Moreover, the overall heat transfer was lower for the nonuniform heating case compared to that for the uniform heating case. The unsteady laminar natural convection flow for saturated porous was illustrated by Hossain and Wilson [8] by using a rectangular enclosure. The non-isothermal left wall, hot bottom wall, cold top, and right walls were used in their work. Results showed that the porosity of the medium increased for the walls with decreasing volumetric flow rate and heat transfer rate of fluid. Song and Viskanta [9] theoretically and experimentally explained the natural convection flow inside a rectangular enclosure partly filled with an anisotropic porous medium. Volume-averaged conservation equations were used to consider the effect of the anisotropic flow characteristics of the porous medium on flow and heat transfer. Natural convection flows in a square cavity filled with a porous matrix was studied by Sathiyamoorthy et al. [10]. The local Nusselt number exhibited an oscillatory nature due to the presence of multiple secondary circulations. The average Nusselt numbers were almost constant through an entire range of Ra up to 10^6 for Da = 10^{-5} owing to the conduction-dominant mode of heat transfer. Bin Kim [11] studied natural convection in a porous square enclosure using the Brinkman-extended Darcy model and noted that the porous region acted as a heat-generating solid block in the conduction-controlling regime. Results showed that an asymptotic convection regime existed where the flow was almost independent of the permeability and conductivity of the porous medium.

Lee [12] numerically and experimentally studied fluid motion and heat transfer in a differentially heated nonrectangular enclosure and reported the effect of aspect ratios, Rayleigh number, inclination of the enclosure on the flow, and thermal characteristics. The highest and lowest values of the average Nusselt number were found at inclination angles of 180° and 270°, respectively. Philip [13] advanced the exact solutions for a small Rayleigh number during free convection in different-shaped enclosures (i.e., elliptical, rectangular, and triangular) due to the uniform temperature gradient. The author concluded that the convective flows were

Received: March 2019, Accepted: August 2019
Correspondence to: Prof. Dr. Isam Mejbel Abed
Faculty of Mechanical Engineering,
University of Babylon, Babylon province, Iraq
E-mail: eng.isam.m@uobabylon.edu.iq
doi: 10.5937/fmet2001082M
© Faculty of Mechanical Engineering, Belgrade. All rights reserved

independent of the cavity orientation at a low value of Rayleigh number. Lyican et al. [14] attempted to study heat transfer by natural convective flow in a trapezoidal enclosure with parallel cylindrical top and bottom walls at different temperatures and adiabatic side walls. Hyun and Choi [15] used the finite difference method to numerically study transient natural convective heat transfer in a parallelogram-shaped enclosure with high Rayleigh numbers. With a parallelogram-shaped enclosure utilized as a transient thermal diode, they identified the importance of tilt angle by using it to control the partition walls of the enclosure. Varol et al. [16] studied natural convection within trapezoidal enclosures partially cooled from the inclined wall and the heat transfer and fluid flow caused by buoyancy forces in divided trapezoidal enclosures. The divider had constant thermal conductivity. Results showed that the conduction mode of heat transfer prevailed within the cavity for low Rayleigh numbers, low thermal conductivity ratio, and high partition thickness.

The effect of nanoparticles on convection heat transfer and fluid flow has been mentioned in several research, such as Alsabery et al. [17], who numerically studied the problem of Darcian natural convection in a trapezoidal cavity partly filled with porous layer and partly with nanofluid layer. Results showed that the addition of Ag–water nanofluid clearly increased the convection, and the inclination angle of the cavity variation had an important effect on heat transfer rate. The effect of nanoparticles on natural convection and entropy generation in a semicircular enclosure filled with nanofluid (Cu water) was presented in Al-Zamily and Amin [18]. Results showed that the heat transfer rate increased with an increase in Rayleigh number and nanoparticle volume fraction. System irreversibility increased as nanoparticle volume fraction increased. Al-Zamily and Amin [19] studied the fluid flow, heat transfer, and entropy generation within a square cavity embedded with heat flux and subject to the horizontal magnetic field. Results revealed that the effect of the Hartmann on Nusselt number increased as the Darcy number increased, especially at high Rayleigh numbers. Moreover, at Ra = 10^7 and Φ = 0.15, the percentage decreased in the Nusselt number owing to the presence of a magnetic field (Ha = 40). The values were 85.89% at Da = 10^{-1}, 87.12% at Da = 10^{-3}, and 98.69% at Da = 10^{-5}. Finally, finite element technique (FET) was used to numerically study natural convection heat transfer within a trapezoidal enclosure filled with Ag nanofluid and saturated porous medium with the same nanofluid.

2. MATHEMATICAL MODEL

The dimensionless Navier–Stokes and energy equations for nanofluid and porous–nanofluid medium within a trapezoidal enclosure was solved numerically using FET. The fluid flow was considered laminar, incompressible, 2-D, and steady without internal heat generation. The thermophysical properties of the nanofluid were assumed to be constant, except for density in the Y-direction of the momentum equation. Local thermal equilibrium along with the Darcy–Brinkman model was used to model the saturated porous medium. Figure 1 illustrates a diagram of the trapezoidal enclosure with an inner adiabatic circular cylinder within. The cavity was subdivided into two layers; the top was filled with Ag nanofluid and the bottom with a saturated porous medium mixed with the same nanofluid. The central bottom length (L_h = 0.5) was considered to maintain isotherm hot temperature while the other length of the bottom wall was kept adiabatic. The two-inclined lines with an angle and the circular cylinder were kept adiabatic.

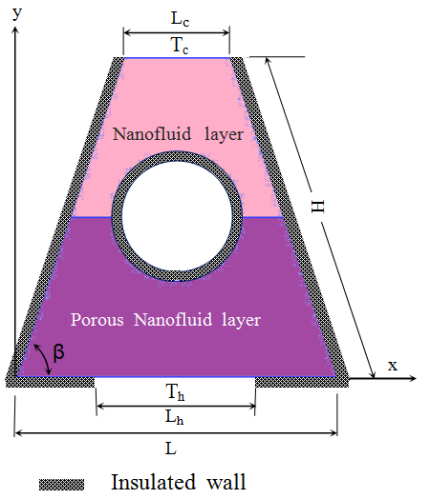

Figure 1. Diagram of the trapezoidal enclosure with an inner adiabatic circular cylinder

2.1 Governing dimensional equations

The equations for the nanofluid represented are as follows [20, 21]:

Continuity

$$\frac{\partial u_{na}}{\partial x}+\frac{\partial v_{na}}{\partial y}=0 \tag{1}$$

X – momentum

$$\rho_{na}\left(u_{na}\frac{\partial u_{na}}{\partial x}+v_{na}\frac{\partial u_{na}}{\partial y}\right)= \tag{2}$$

$$=-\frac{\partial p}{\partial x}+\mu_{na}\left(\frac{\partial^2 u_{na}}{\partial x^2}+\frac{\partial^2 u_{na}}{\partial y^2}\right)$$

Y – momentum

$$\rho_{na}\left(u_{na}\frac{\partial v_{na}}{\partial x}+v_{na}\frac{\partial v_{na}}{\partial y}\right)+ \tag{3}$$

$$=-\frac{\partial p}{\partial y}+\mu_{na}\left(\frac{\partial^2 v_{na}}{\partial x^2}+\frac{\partial^2 v_{na}}{\partial y^2}\right)$$

Energy

$$u_{na}\frac{\partial T_{na}}{\partial x}+v_{na}\frac{\partial T_{na}}{\partial y}=\frac{\alpha_{na}}{\alpha_{fl}}\left(\frac{\partial^2 T_{na}}{\partial x^2}+\frac{\partial^2 T_{na}}{\partial y^2}\right) \tag{4}$$

The governing equations for the porous media partition [19] are as follows:

Continuity

$$\frac{\partial u_{po}}{\partial x}+\frac{\partial v_{po}}{\partial y}=0 \tag{5}$$

$X-momentum$

$$\rho_{na}\left(u_{po}\frac{\partial u_{po}}{\partial x}+v_{po}\frac{\partial u_{po}}{\partial y}\right)=$$

$$=-\varepsilon^2\frac{\partial p}{\partial x}+\varepsilon\mu_{na}\left(\frac{\partial^2 u_{po}}{\partial x^2}+\frac{\partial^2 u_{po}}{\partial y^2}\right)- \tag{6}$$

$$-\varepsilon^2\frac{\mu_{na}}{k}u_{po}$$

$Y-momentum$

$$\rho_{na}\left(u_{po}\frac{\partial v_{po}}{\partial x}+v_{po}\frac{\partial v_{po}}{\partial y}\right)-\varepsilon^2\frac{\partial p}{\partial y}+$$

$$+\varepsilon\mu_{na}\left(\frac{\partial^2 v_{po}}{\partial x^2}+\frac{\partial^2 v_{po}}{\partial y^2}\right)- \tag{7}$$

$$-\varepsilon^2\frac{\mu_{na}}{k}v_{po}+\beta_{na}\rho_{na}g\left(T_{na}-T_c\right)$$

$Energy$

$$u_{po}\frac{\partial T_{po}}{\partial x}+v_{po}\frac{\partial T_{po}}{\partial y}=\alpha_{eff}\left(\frac{\partial^2 T_{po}}{\partial x^2}+\frac{\partial^2 T_{po}}{\partial y^2}\right) \tag{8}$$

where ρ is the density, α is the thermal diffusifity, μ is the dynamic viscosity, ε is the porosity, K is the permeability, β is the thermal expansion coefficient, and *na, po*, and *fl* are the subscripts for nanofluid, porous medium, and pure fluid, respectively.

Suppose the relation for stream function $\left(u=\frac{\partial\psi}{\delta y}\right)$, $\left(v=-\frac{\partial\psi}{\delta x}\right)$, and vorticity $\left(\omega=\frac{\partial v}{\partial x}-\frac{\partial u}{\partial y}\right)$ are presented in the dimensionless parameters as follows:

$$\mathrm{X}=\frac{x}{L};Y=\frac{y}{L};U=\frac{uL}{\alpha_{fl}};V=\frac{vL}{\alpha_{fl}};P=\frac{pL^2}{\rho_{na}{\alpha_f}^2};$$

$$\mathrm{Da}=\frac{k_{fl}}{L^2};\theta=\frac{T-T_c}{T_h-T_c}$$

$$Ra=\frac{g\beta_{fl}(T_h-T_c)L^3}{\nu_{fl}\alpha_{fl}};Pr=\frac{\nu_{fl}}{\alpha_{fl}},\Psi=\frac{\psi}{\alpha_{fl}},\Omega=\frac{\omega L^2}{\alpha_{fl}}$$

The physical properties of the nanofluid can be expressed as follows [22]:

$$\rho_{na}=(1-\varphi)\rho_{fl}+\varphi\rho_{po} \tag{9}$$

$$(\rho\beta)_{na}=(1-\varphi)(\rho\beta)_{fl}+\varphi(\rho\beta)_{po} \tag{10}$$

$$\alpha_{na}=\frac{K_{na}}{(\rho c_p)_{na}} \tag{11}$$

$$\alpha_{eff}=\frac{K_{eff}}{(\rho c_p)_{na}} \tag{12}$$

$$K_{eff}=(1-\varepsilon)K_s+\varepsilon K_{na} \tag{13}$$

$$(\rho c_p)_{na}=(1-\varphi)\left(\rho c_p\right)_{fl}+\varphi(\rho c_p)_{po} \tag{14}$$

$$K_{na}=K_{fl}\frac{\left(K_{po}+2K_{fl}\right)-2\varphi\left(K_{fl}-K_{po}\right)}{\left(K_{po}+2K_{fl}\right)+\varphi\left(K_{fl}-K_{po}\right)} \tag{15}$$

$$\mu_{na}=\mu_{fl}/(1-\varphi)\text{\^{}}2.5 \tag{16}$$

The dimensionless equations take the following forms:

$Continuity$

$$\frac{\partial U_{na}}{\partial X}+\frac{\partial V_{na}}{\partial Y}=0 \tag{17}$$

$X-momentum$

$$U_{na}\frac{\partial U_{na}}{\partial X}+V_{na}\frac{\partial U_{na}}{\partial Y}= \tag{18}$$

$$=-\frac{\partial P}{\partial X}+\frac{Pr}{(1-\varphi)^{2.5}}\frac{\rho_{fl}}{\rho_{na}}\left(\frac{\partial^2 U_{na}}{\partial X^2}+\frac{\partial^2 U_{na}}{\partial Y^2}\right)$$

$Y-momentum$

$$U_{na}\frac{\partial V_{na}}{\partial X}+V_{na}\frac{\partial V_{na}}{\partial Y}=$$

$$=-\frac{\partial P}{\partial Y}+\frac{Pr}{(1-\varphi)^{2.5}}\frac{\rho_{fl}}{\rho_{na}}\left(\frac{\partial^2 V_{na}}{\partial X^2}+\frac{\partial^2 V_{na}}{\partial Y^2}\right)+ \tag{19}$$

$$+\frac{(\rho\beta)_{na}}{\rho_{na}\beta_{fl}}RaPr\theta_{na}$$

$Energy$

$$U_{na}\frac{\partial\theta_{na}}{\partial X}+V_{na}\frac{\partial\theta_{na}}{\partial Y}=\frac{\alpha_{na}}{\alpha_{fl}}\left(\frac{\partial^2\theta_{na}}{\partial X^2}+\frac{\partial^2\theta_{na}}{\partial Y^2}\right) \tag{20}$$

The dimensionless form of the governing equations for the porous media domain will be written as:

$$\frac{\partial U_{po}}{\partial X}+\frac{\partial V_{po}}{\partial Y}=0 \tag{21}$$

$X-momentum$

$$\mathrm{U_{po}}\frac{\partial \mathrm{U_{po}}}{\partial \mathrm{X}}+\mathrm{V_{po}}\frac{\partial \mathrm{U_{po}}}{\partial \mathrm{Y}}=-\frac{\partial \mathrm{P}}{\partial \mathrm{X}}+$$

$$+\frac{\mathrm{Pr}}{(1-\varphi)^{2.5}}\frac{\rho_{\mathrm{fl}}}{\rho_{\mathrm{na}}}\left(\frac{\partial^2 \mathrm{U_{po}}}{\partial \mathrm{X}^2}+\frac{\partial^2 \mathrm{U_{po}}}{\partial \mathrm{Y}^2}\right)- \tag{22}$$

$$-\frac{\mathrm{Pr}}{(1-\varphi)^{2.5}}\frac{\rho_{\mathrm{fl}}}{\rho_{\mathrm{na}}}\frac{\mathrm{U_{po}}}{\mathrm{Da}}$$

$Y-momentum$

$$\mathrm{U_{po}}\frac{\partial \mathrm{V_{po}}}{\partial \mathrm{X}}+\mathrm{V_{po}}\frac{\partial \mathrm{V_{po}}}{\partial \mathrm{Y}}=-\frac{\partial \mathrm{P}}{\partial \mathrm{Y}}+$$

$$+\frac{\mathrm{Pr}}{(1-\varphi)^{2.5}}\frac{\rho_{\mathrm{fl}}}{\rho_{\mathrm{na}}}\left(\frac{\partial^2 \mathrm{V_{po}}}{\partial \mathrm{X}^2}+\frac{\partial^2 \mathrm{V_{po}}}{\partial \mathrm{Y}^2}\right)- \tag{23}$$

$$-\frac{\mathrm{Pr}}{(1-\varphi)^{2.5}}\frac{\rho_{\mathrm{fl}}}{\rho_{\mathrm{na}}}\frac{\mathrm{V_{po}}}{\mathrm{Da}}+\frac{(\rho\beta)_{\mathrm{na}}}{\rho_{\mathrm{na}}\beta_{\mathrm{fl}}}\mathrm{RaPr}\theta_{\mathrm{P0}}$$

Energy

$$U_{po}\frac{\partial\theta_{po}}{\partial X}+V_{po}\frac{\partial\theta_{po}}{\partial Y}=\frac{\alpha_{na}}{\alpha_{fl}}\left(\frac{\partial^2\theta_{po}}{\partial X^2}+\frac{\partial^2\theta_{po}}{\partial Y^2}\right) \quad (24)$$

The boundary conditions on the outside walls of the enclosure are shown in Table 1.

Table 1. Boundary conditions for the enclosure

Position	Direction	U, V, Ψ	θ
Left side wall	Y = H	0, 0, 0	$\frac{\partial\theta}{\partial n}=0$
Right side wall	Y = H	0, 0, 0	$\frac{\partial\theta}{\partial n}=0$
Bottom wall	X = L-L_h	0, 0, 0	$\frac{\partial\theta}{\partial Y}=0$
Bottom wall	X = L_h	0, 0, 0	1
Top wall	X = L_c	0, 0, 0	0

The thermo-physical properties of the Ag nanofluid are shown in Table 2.

Table 2. Properties of pure water and Cu nanoparticles as presented in Ref. [23]

Properties	C_p (J/kg·k)	ρ (kg/m^3)	k (W/m·k)	B (1/k)	μ (kg/m·s)
Ag	235	10500	429	1.89×10^{-5}	-
Pure water	4179	997.1	0.613	21×10^{-5}	0.000372

The conditions applied to the permeable surfaces between the porous partition and nanofluid can be defined as:

$$\theta_{po}=\theta_{na},\frac{\partial\theta_{na}}{\partial X}=\frac{K_{eff}}{K_{na}}\frac{\partial\theta_{po}}{\partial X},$$
$$\Psi_{po}=\Psi_{na},\frac{\partial\Psi_{na}}{\partial X}=\frac{\partial\Psi_{po}}{\partial X},$$
$$\Omega_{po}=\Omega_{na},\frac{\partial\Omega_{na}}{\partial X}=\frac{\partial\Omega_{po}}{\partial X} \quad (25)$$
$$\mu_{po}\left(\frac{\partial U_{po}}{\partial Y}+\frac{\partial V_{po}}{\partial X}\right)=\mu_{na}\left(\frac{\partial U_{na}}{\partial Y}+\frac{\partial V_{na}}{\partial X}\right),$$
$$P_{po}=P_{na},\quad\frac{\partial P_{po}}{\partial X}=\frac{\partial P_{na}}{\partial Y}$$

The local and average Nusselt numbers for the hot wall are determined as follows:

$$Nu_{local}=\frac{K_{na}}{K_{fl}}\frac{1}{\pi}\frac{\partial\theta}{\partial n} \quad (26)$$

$$Nu_{ave}=\frac{K_{na}}{K_{fl}}\int_0^1\frac{\partial\theta}{\partial n}dy \quad (27)$$

2.2 Validation

To ensure the accuracy of the present work, the numerical results were validated with those of Kim et al. [1] in terms of streamlines and isotherms for the inner cylinder located inside a square enclosure filled with air as a working fluid (Figure 2).

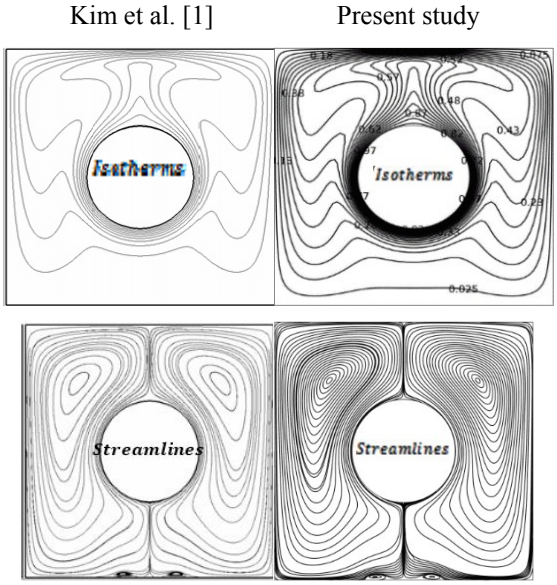

Figure 2. Validation solution for the present work with reference to Kim et al. [1]

The numerical grid generation is presented in Figure 3, which also illustrates a triangular fine mesh for the trapezoidal enclosure.

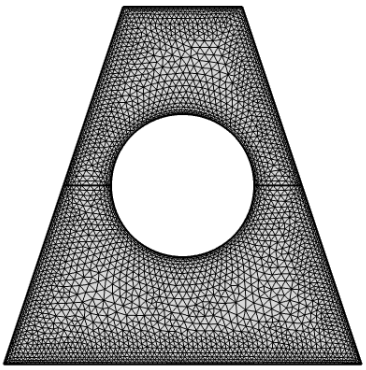

Figure 3. Numerical grid generation for the circular cylinder inside the trapezoidal enclosure

3. RESULTS AND DISCUSSION

3.1 Influence of Rayleigh number

This section discusses the influence of Rayleigh number on streamlines and isotherms for saturated porous medium–Ag nanofluid (lower layer) with the same nanofluid (upper layer) at (Da = 0.001, φ = 0.1, Y_P = 0.5). Figure 4a shows that when the Rayleigh number increased from Ra = 10^4 to Ra = 10^6, the maximum absolute value of stream function increased from $|\Psi_{max}|$ = 0.015405 to $|\Psi_{max}|$ = 3.6520, respectively. The physical reason is due to the improving fluid flow strength and intensity as the Rayleigh number increased. The convection heat transfer is dominated at high Rayleigh number values, which lead to increased stream function.

For the isotherm contours, Figure 4b shows that when the Rayleigh number is low, the isotherms have horizontal uniform shapes due to the dominated

conduction heat transfer and the weak influence of convection fluid flow. However, when the Rayleigh number is low (Ra = 10^6), a clear change in isotherm contours can be noted. The isotherm shapes change their behavior from the horizontal pattern into the curved pattern. In this case, the convective heat transfer mode is dominated.

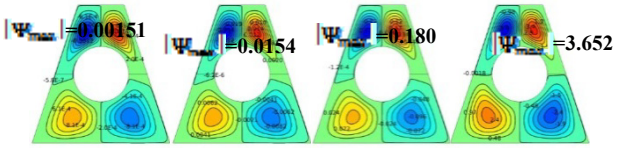

Ra = 10^3 Ra = 10^4 Ra = 10^5 Ra = 10^6

Figure 4a.

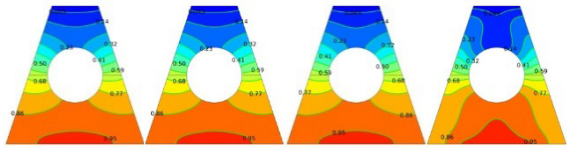

Figure 4b.

Figure 4. Streamlines for trapezoidal enclosure (a) and isotherm (b) contours for various values of the Rayleigh number at (Da = 0.001, □ = 0.1, Y_P = 0.5)

3.2 Influence of Darcy number and nanofluid loading

The effect of Darcy number on the streamlines and isotherms is illustrated in Figures 5a and 5b, respectively, the streamlines and the isotherm contours for saturated porous medium–Ag nanofluid (lower layer) and Ag nanofluid (upper layer) for different values of Darcy numbers at Ra = 10^6, φ = 0.1, and Y_P = 0.5. As the Darcy number increased, the maximum absolute value of the stream function likewise increased. For example, when the Darcy number increased from Da = 10^{-5} to Da = 0.01, the maximum absolute value of the stream function improved from $|\psi_{max}|$ = 4.66e-^{4} to $|\psi_{max}|$ = 6.1018 due to the increase in fluid flow activity. Figure 4a also shows that an increasing Darcy number improves the permeability of the porous medium. Thus, more Ag nanofluid is allowed to penetrate the saturated porous layer and, as a result, the strength of the cell is increased significantly. The effect of heat source on isothermal lines for a nanofluid with four values of Darcy numbers at Ra = 10^6, φ = 0.1, and Y_P = 0.5 is discussed.

Figure 5a

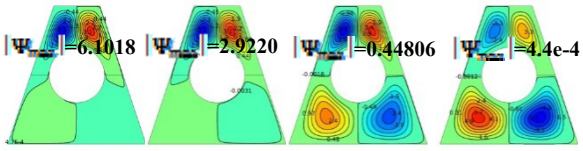

Da = 0.01 Da = 0.001 Da = 1e-4 Da = 1e-5

Figure 5b

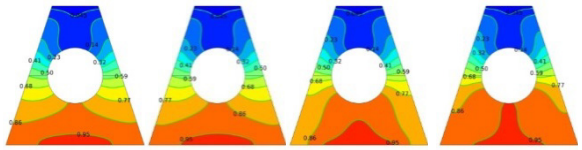

Figure 5. Streamlines for trapezoidal enclosure (a) and isotherm contours (b) for various values of Da number at Ra = 10^6, □ = 0.1, and Y_P = 0.5

When the Darcy number increases from Da = 10^{-5} to Da = 0.01, the maximum absolute value of the isothermal lines becomes denser around the heat source and reaches a maximum value at hot wall 0.95 and minimum value at cold wall 0.045. This outcome is attributed to the increase in fluid flow activity as the Darcy number increases. In this case, the thickness of the boundary layer caused by aggregation of isothermal lines around the heat source decreases; thus, the heat transfer rate is enhanced.

3.3 Influence of porous layer thickness

Figure 6 displays the influence of vertical changes in the porous layer thickness on fluid flow strength and isotherm contours at Ra = 10^6, Da = 0.001, and Ø = 0.1. When the porous layer thickness increases from Y_p = 0.2 to Y_p = 0.8, the maximum absolute value of stream function decreases from $|\psi_{max}|$ = 4.6054 to $|\psi_{max}|$ = 2.66 due to the resistance of the porous layer hydrodynamic.

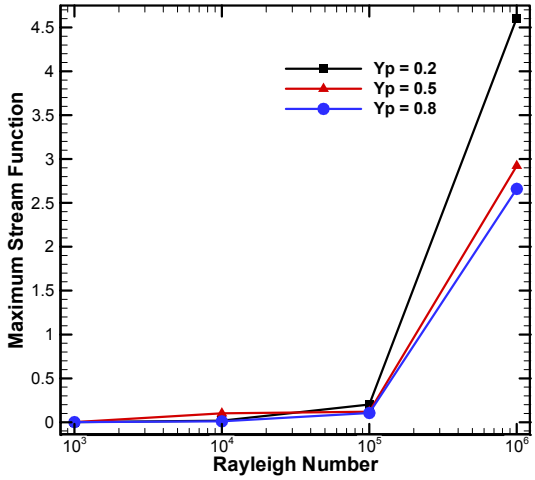

Figure 6a. Maximum stream function versus Rayleigh number for various porous layer thicknesses

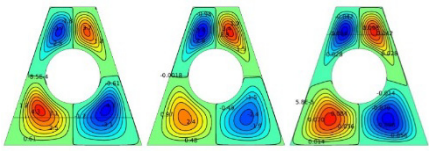

Figure 6b.

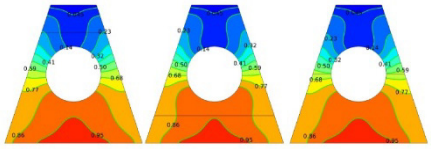

Figure 6c.

Figure 6: Streamlines for trapezoidal enclosure (b) and isotherm contours (c) for various values of Da number at Ra = 10^6, □ = 0.1, and Y_P = 0.5

3.4 Influence of Nusselt Number

Figure 7 shows the profile of local Nusselt numbers along the adiabatic circular cylinder at various volume fractions at Ra = 10^6, Da = 0.001, and Y_p = 0.8. The trend is shaped like the sinusoidal function. Decreased Nusselt numbers along the arc length until reaching

minimum value approach 0 when the arc length is less than 0.5 and then reach the maximum approach of 3 when the arc length is more than 0.5. Figure 8 explains the average Nu with Ra at various nanofluid volume fractions. The value of the Nusselt number increases when the nanoparticle volume fraction is increased because of an increase in the thermal conductivity, viscosity, and, density of the nanofluid. Figure 9 shows Nu with Da at various nanofluid volume fractions; when the nanofluid is increased, an increase in the Nusselt number is observed. In addition, an increased Darcy number causes the Nusselt number to increase as well due to an increase in the thermal conductivity, viscosity, and, density of the nanofluid.

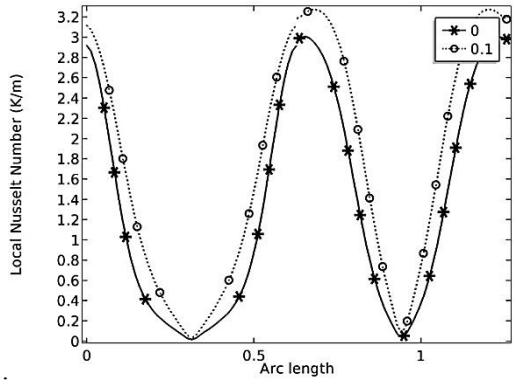

Figure 7. Local Nusselt number along the adiabatic circular cylinder at various volume fractions at Ra = 10^6, Da = 0.001, and Y_p = 0.8

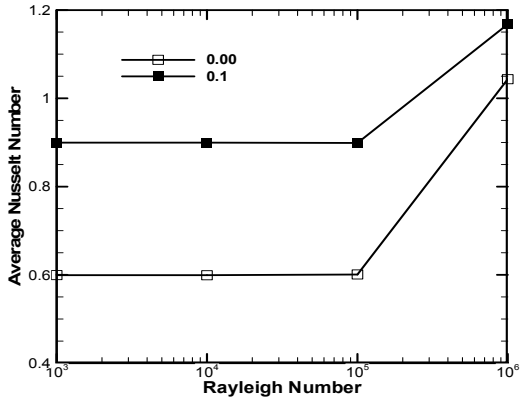

Figure 8. Average Nu with Ra at various nanofluid volume fractions

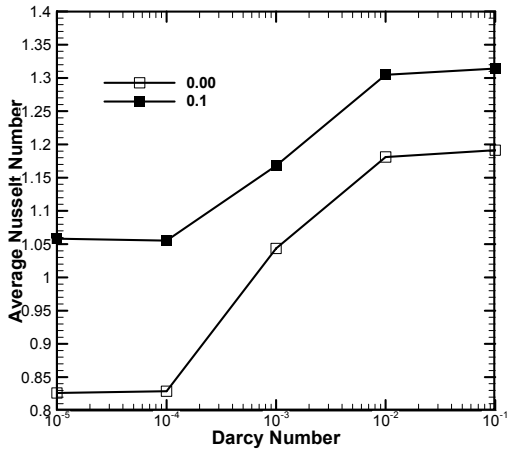

Figure 9. Average Nu with Da at various nanofluid volume fractions

Figure 10 shows the profile of average Nusselt numbers Ra for various Darcy numbers. An increase in Nusselt number is observed with the increased Darcy number due to the increasing thermal conductivity. Figure 11 shows the profile of local Nusselt numbers along the adiabatic circular cylinder at various volume fractions at Ra = 10^6, Da = 0.001, and Yp = 0.2, 0.5, and 0.8. Decreased Nusselt numbers along the arc length until they reached minimum value approach 0 when the arc length is less than 0.5 and then reach the maximum approach of 3 when the arc length is more than 0.5. An increased Yp also causes the Nusselt number to increase.

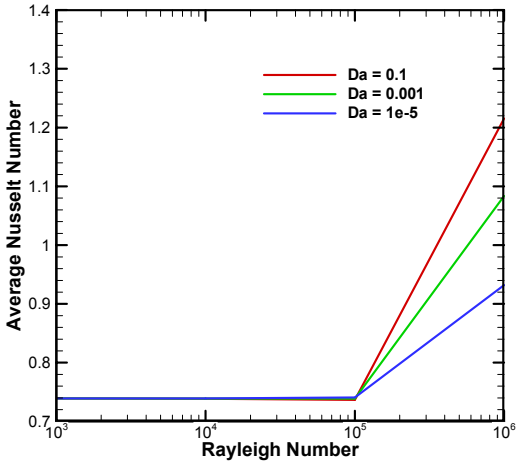

Figure 10. Average Nu with Ra at different Da numbers

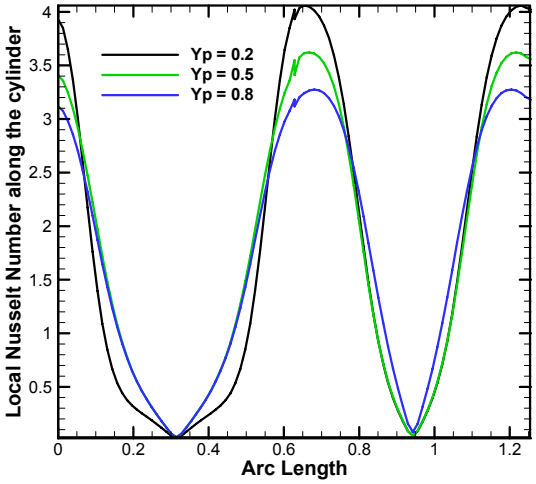

Figure 11. Local Nusselt Number along the adiabatic circular cylinder at various volume fractions at Ra = 10^6, Da = 0.001, Y_p = 0.2, 0.5 and 0.8

4. CONCLUSIONS

On the basis of an overview of the results, the following items can be concluded:

- When the Darcy number is increased from Da = 10^{-5} to Da = 0.01, the maximum absolute value of the stream function improves.
- When the Rayleigh number is increased from Ra = 10^3 to Ra = 10^6, the maximum absolute value of stream function increases.
- At high Rayleigh numbers, values of the natural convection and buoyancy force become dominated, which leads to an increasing stream function.

- The maximum absolute value of the isothermal lines become denser around the heat source. Thus, the value will reach its maximum at the hot wall and its minimum at the cold wall.
- When the thickness of the boundary layer around the heat source decreases, the heat transfer rate is enhanced owing to the aggregation of isothermal lines.

REFERENCES

[1] Kim, B., et al., A numerical study of natural convection in a square enclosure with a circular cylinder at different vertical locations. International Journal of Heat and Mass Transfer, 2008. 51(7-8): p. 1888-1906.

[2] Sudarmadji, S., et al., Effects of cooling process of Al2O3-water nanofluid on convective heat transfer. FME Transactions, 2014. 42(2): p. 155-160.

[3] Ali, F.H., H.K. Hamzah, A. Abdulkadhim, Numerical study of mixed convection nanofluid in an annulus enclosure between outer rotating cylinder and inner corrugation cylinder. Heat Transfer—Asian Research, 2019. 48(1): p. 343-360.

[4] Soltani-Tehrani, A., M.R. Tavakoli, and M.R. Salimpour, Using porous media to improve the performance of a wavy-tube heat exchanger. FME Transactions, 2018. 46(4): p. 631-635.

[5] Aydin, O., A. Ünal, and T. Ayhan, Natural convection in rectangular enclosures heated from one side and cooled from the ceiling. International Journal of Heat and Mass Transfer, 1999. 42(13): p. 2345-2355.

[6] Basak, T., S. Roy, and A. Balakrishnan, Effects of thermal boundary conditions on natural convection flows within a square cavity. International Journal of Heat and Mass Transfer, 2006. 49(23-24): p. 4525-4535.

[7] Kaluri, R.S. and T. Basak, Analysis of distributed thermal management policy for energy-efficient processing of materials by natural convection. Energy, 2010. 35(12): p. 5093-5107.

[8] Hossain, M.A. and M. Wilson, Natural convection flow in a fluid-saturated porous medium enclosed by non-isothermal walls with heat generation. International Journal of Thermal Sciences, 2002. 41(5): p. 447-454.

[9] Song, M. and R. Viskanta, Natural convection flow and heat transfer within a rectangular enclosure containing a vertical porous layer. International journal of heat and mass transfer, 1994. 37(16): p. 2425-2438.

[10] Sathiyamoorthy, M., et al., Steady natural convection flow in a square cavity filled with a porous medium for linearly heated side wall (s). International Journal of Heat and Mass Transfer, 2007. 50(9-10): p. 1892-1901.

[11] Bin Kim, J.M.H., Ho Sang Kwak, Gi, Buoyant convection in a square cavity partially filled with a heat -generating porous medium. Numerical Heat Transfer: Part A: Applications, 2001. 40(6): p. 601-618.

[12] Lee, T., Computational and experimental studies of convective fluid motion and heat transfer in inclined non-rectangular enclosures. International journal of heat and fluid flow, 1984. 5(1): p. 29-36.

[13] Philip, J., Free convection at small Rayleigh number in porous cavities of rectangular, elliptical, triangular and other cross-sections. International Journal of Heat and Mass Transfer, 1982. 25(10): p. 1503-1509.

[14] Iyican, L., Y. Bayazitoglu, and L.C. Witte, An analytical study of natural convective heat transfer within a trapezoidal enclosure. Journal of Heat Transfer, 1980. 102(4): p. 640-647.

[15] Hyun, J.M. and B.S. Choi, Transient natural convection in a parallelogram-shaped enclosure. International Journal of Heat and Fluid Flow, 1990. 11(2): p. 129-134.

[16] Varol, Y., H.F. Oztop, and I. Pop, Natural convection in right-angle porous trapezoidal enclosure partially cooled from inclined wall. International Communications in Heat and Mass Transfer, 2009. 36(1): p. 6-15.

[17] Alsabery, A., et al., Darcian Natural Convection in an Inclined Trapezoidal Cavity Partly Filled with a Porous Layer and Partly with a Nanofluid Layer. Sains Malaysiana, 2017. 46(5): p. 803-815.

[18] Al-Zamily, A. and M.R. Amin, Natural convection and entropy generation in a nanofluid-filled semi-circular enclosure with heat flux source. Procedia Engineering, 2015. 105: p. 418-424.

[19] Al-Zamily, A. and M.R. Amin. Natural convection and entropy generation in a cavity filled with two horizontal layers of nanofluid and porous medium in presence of a magnetic field. in ASME 2015 International Mechanical Engineering Congress and Exposition. 2015. American Society of Mechanical Engineers.

[20] Al-Zamily, A.M.J., Analysis of natural convection and entropy generation in a cavity filled with multi-layers of porous medium and nanofluid with a heat generation. International Journal of Heat and Mass Transfer, 2017. 106: p. 1218-1231.

[21] Hussain, S.H. and M.S. Rahomey, Comparison of Natural Convection Around a Circular Cylinder With Different Geometries of Cylinders Inside a Square Enclosure Filled With Ag-Nanofluid Superposed Porous-Nanofluid Layers. Journal of Heat Transfer, 2019. 141(2): p. 022501.

[22] Chamkha, A.J. and M.A. Ismael, Conjugate heat transfer in a porous cavity filled with nanofluids and heated by a triangular thick wall. International Journal of Thermal Sciences, 2013. 67: p. 135-151.

ДОВОЂЕЊЕ ТОПЛОТЕ ПРИРОДНОМ КОНВЕКЦИЈОМ ЗА АДИЈАБАТСКИ КРУЖНИ ЦИЛИНДАР СМЕШТЕН УНУТАР ТРАПЕЗОИДНОГ КУЋИШТА ИСПУЊЕНОГ НАНОФЛУИДОМ СУПЕРПОНИРАНИМ СА СЛОЈЕМ ПОРОЗНОГ НАНОФЛУИДА

И.М. Абед, А. Абдулкадим, Р.А. Хамза, Х.К. Хамза, Ф.Х. Али

Нумеричким поступком се истражује довођење топлоте природним путем за кружни цилиндар са адијабатским зидовима који је смештен унутар трапезоидног кућишта испуњеног нанофлуидом на бази сребрне воде, суперпонираним са слојем засићеног порозног нанофлуида. Зид на дну кућишта се делимично загрева изотермном високом температуром а изотермна ниска тепература се одржава на зиду на врху кућишта.

Техника коначних елемената се користи за нумеричко израчунавање бездимензионих Навијер-Стоксових једначина нанофлуида и порозног нанофлуида између цилиндра и кућишта. Прецизност програма је проверена поређењем резултата за струјнице и изотерме добијених нумеричким путем са резултатима Кима и сар. (2008). Утврђен је висок степен слагања између резултата добијених у овом раду и резултата Кима и сар. Истраживање је обухватило следеће параметре: Рејлијев број, Дарсијев број, запремински удео наночестица и дебљину порозног слоја.